Lithium Storage in Li4Ti5O12 Spinel: The Full Static Picture from Electron Microscopy

ARTICLE *in* ADVANCED MATERIALS · JUNE 2012

Impact Factor: 17.49 · DOI: 10.1002/adma.201200450 · Source: PubMed

12 AUTHORS, INCLUDING:

Xia Lu
McGill University
23 PUBLICATIONS **852** CITATIONS
SEE PROFILE

Hong Li
Chinese Academy of Sciences
273 PUBLICATIONS **10,131** CITATIONS
SEE PROFILE

Zhaoxiang Wang
Chinese Academy of Sciences
166 PUBLICATIONS **5,201** CITATIONS
SEE PROFILE

Yuichi Ikuhara
The University of Tokyo
478 PUBLICATIONS **5,751** CITATIONS
SEE PROFILE

Lithium Storage in $Li_4Ti_5O_{12}$ Spinel: The Full Static Picture from Electron Microscopy

Xia Lu, Liang Zhao, Xiaoqing He, Ruijuan Xiao, Lin Gu, Yong-Sheng Hu,* Hong Li, Zhaoxiang Wang, Xiaofeng Duan, Liquan Chen, Joachim Maier, and Yuichi Ikuhara*

Lithium-ion batteries (LIBs) have been considered the most promising storage device for electric vehicles and large-scale energy storage.[1–3] The spinel $Li_4Ti_5O_{12}$, used as a model material here, is an important anode for long-life LIBs. It can be crystallographically more precisely described as $[Li]_{8a}[Li_{1/3}Ti_{5/3}]_{16d}[O_4]_{32e}$ or even as $[Li]_{8a\ 16c}[Ti]_{16d}[Li_{1/3}Ti_{2/3}]_{16d}[O_4]_{32e}$ (where a blank indicates a vacancy).[4–8] The former formula indicates its atomic occupations, with three out of four Li^+ ions occupying the 8a sites, the remaining Li^+ and all titanium ions being in the 16d sites, and the oxygen ions in the 32e sites. The latter specifically indicates the 16c structural vacancies into which the Li^+ ions will insert during the discharge process.[9–19] According to the literature,[12,13] this Li insertion into the 16c sites is accompanied by Li^+ ion transfer from the 8a sites to the 16c sites, leading to the phase transition from the spinel structure $[Li]_{8a\ 16c}[Ti]_{16d}[Li_{1/3}Ti_{2/3}]_{16d}[O_4]_{32e}$ to the rock-salt structure $_{8a}[Li_2]_{16c}[Ti]_{16d}[Li_{1/3}Ti_{2/3}]_{16d}[O_4]_{32e}$, in which the 8a site is empty.

This mechanism has not been investigated by direct visualization. Furthermore, as a typical two-phase reaction, direct observation of the interface has not yet been successful. In spite of experimental and modeling work performed so far,[14–25] there is still no direct evidence that would lead to a clear picture of Li storage in $Li_4Ti_5O_{12}$ and the interfacial structure formed in the two-phase transition reaction.

Atomic imaging of light elements by microscopy techniques has brought about significant progress.[26–39] In particular, spherical aberration-corrected scanning transmission electron microscopy (STEM) has showed its potential not only for mapping oxygen defects (e.g., in grain boundaries[29]), but also for the light elements Li[32] and H.[33] Recent examples are the detection of the Li-Fe anti-site disorder in $LiFePO_4$,[30] the staging phenomenon in delithiated $LiFePO_4$,[34,39] and Li^+ ion distributions in the cathode[31,35,36] as well as in the anode.[37]

In this Communication, the STEM technique is employed, in combination with first-principles calculations, i) to elucidate Li^+ rearrangements on lithiated-$Li_4Ti_5O_{12}$ electrodes in addition to the Li^+ ion distribution in $Li_4Ti_5O_{12}$, ii) to investigate the phase boundary involved in this presumably topotactic two-phase reaction, and iii) to investigate the electronic charge distribution after lithiation. The results are very revealing; they not only clearly corroborate the above described structural features by direct visualization, they also show the occurrence of a very sharp, dislocation-free coherent heterophase boundary. Moreover, two different chemical states, Ti^{3+} and Ti^{4+}, are derived from atomic-scale electron energy loss spectroscopy (EELS). On lithiation, only 3/5 titanium, not only on the average but referring to crystallographically clearly distinguishable sites, are reduced to Ti^{3+} while the others still stay in Ti^{4+} states when the $Li_4Ti_5O_{12}$ electrode is discharged to 1.0 V. These sites are neighbors to the excess Li introduced, indicating strong Li^+–e^- association. This is consistent with general gradient approximation (GGA) functional plus U (GGA+U) calculations based on density functional theory (DFT) and also with the previous defect chemical considerations for $LiFePO_4$[40] and TiO_2.[41]

We begin with identification of the Li and Ti columns in $Li_4Ti_5O_{12}$. In general, the STEM technique is capable of spatial sub-angstrom resolution.[29–39] It is noteworthy that the contrast of the high-angle annular-dark-field (HAADF) image exhibits a $Z^{1.7}$ dependence as compared with $Z^{1/3}$ for the annular-bright-field (ABF) image with respect to the atomic number Z.[42,43] **Figure 1** shows the $Li_4Ti_5O_{12}$ lattice and the corresponding HAADF and ABF STEM images viewed along the [110] direction (Figures S5–S12 in the Supporting Information; simulated ABF images in Figure S6). The average size of $Li_4Ti_5O_{12}$ is 5 μm. These are agglomerates of smaller (100 nm) grains (Figure S2, Supporting Information). The different atomic columns are clearly revealed based on the contrast in Figures 1b and c. By comparing the repeat unit (red quadrilateral) in Figure 1b with Figure 1a, the 32e oxygen sites and 16d titanium sites can be clearly seen in the HAADF image, as shown in the left-hand small panel, which is consistent with the atomic occupancies in Figure 1a. The different contrast in Figure 1b also clearly reveals two different titanium columns. The strong white spots (Ti_a arrays) have a longer interval along the $[\bar{1}10]$ direction than weak white spots (Ti_b arrays). Note that the Ti content in Ti_a columns is roughly twice that in the Ti_b

X. Lu, L. Zhao, X. He, Dr. R. J. Xiao, Prof. L. Gu, Prof. Y.-S. Hu, Prof. H. Li, Prof. Z. X. Wang, Prof. X. F. Duan, Prof. L. Q. Chen
Beijing National Laboratory for Condensed Matter Physics
Institute of Physics
Chinese Academy of Sciences, Beijing 100190, P. R. of China
E-mail: yshu@aphy.iphy.ac.cn; l.gu@aphy.iphy.ac.cn
Prof. L. Gu, Y. Ikuhara
WPI Advanced Institute for Materials Research
Tohoku University
Sendai 980-8577, Japan
Prof. L. Gu, Y. Ikuhara
Nanostructures Research Laboratory
Japan Fine Ceramic Centre, Nagoya 456-8587, Japan
Prof. J. Maier
Max Planck Institute for Solid State Research
70569 Stuttgart, Germany
Prof. Y. Ikuhara
Institute of Engineering Innovation
The University of Tokyo Tokyo 113-8654 Japan

DOI: 10.1002/adma.201200450

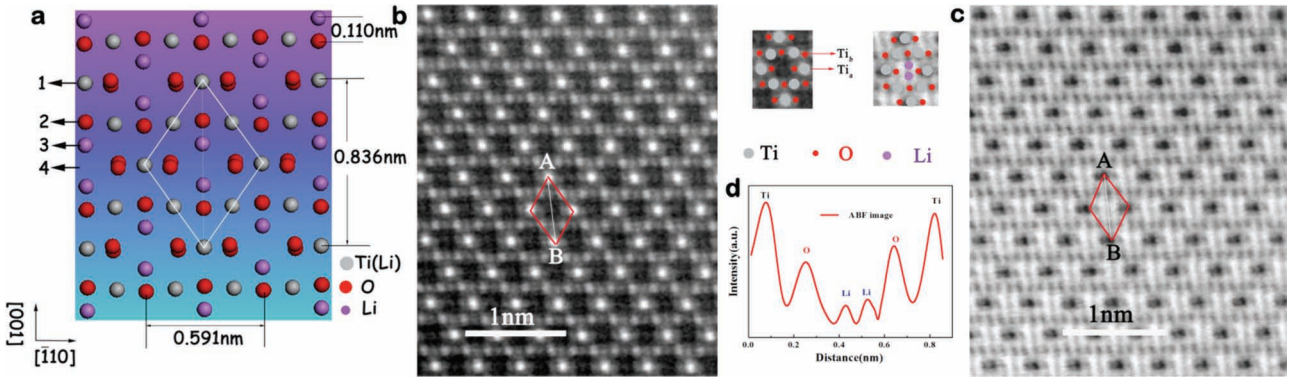

Figure 1. Lattice and STEM images for $Li_4Ti_5O_{12}$ along the [110] zone axis. a) Schematic lattice of $Li_4Ti_5O_{12}$. The labels 1, 2, 3, and 4 at the left of (a), which is the view along the [110] direction, correspond to the 16d, 32e, 8a, and 16c (vacancy) sites in the $Li_4Ti_5O_{12}$ lattice. b,c) Enlarged HAADF (b) and ABF (c) images of $Li_4Ti_5O_{12}$. d) The corresponding line profile from the ABF image. Note that the image contrast of the dark dots is inverted and displayed as peaks.

columns, giving a random distribution of 16d Li^+ ion sites when viewed along the [110] direction.

From the ABF image in Figure 1c, the 8a Li^+ ion columns can be visualized as shown in the right-hand small panel, in addition to the oxygen and titanium columns. The stability of Li^+ ions in 8a sites is corroborated by means of DFT calculations (for the method see the Supporting Information). The DFT results show that the lower energy configuration (Table S1 in the Supporting Information) corresponds to all Li^+ ions occupying 8a sites, rather than other sites in the $Li_4Ti_5O_{12}$ supercell (Figure S13 in the Supporting Information). Nevertheless, there are still site fluctuations on the Li^+ ion columns due to thermodynamic vibrations at elevated temperature. The Li–Li distances in the ABF micrograph are slightly shorter than those in the lattice (Figure 1a and Figure S6 in the Supporting Information) along the [110] direction. However, the corresponding line profiles, with two pronounced Li^+ ion peaks, can obviously distinguish the Li^+ ions in 8a sites as shown in Figure 1d. (It is interesting to note that an irregular outmost surface layer, ca. 2 nm thick and totally different from the interior part, is always found in $Li_4Ti_5O_{12}$ surface layers (Figures S5 and S10 in the Supporting Information). The contrast of Li^+ ion columns can hardly be identified in this outmost surface region, which is quite probably related to titanium-rich compositions, and could be responsible for the gas-releasing issues (package swelling) when $Li_4Ti_5O_{12}$ is used as an anode in a real battery.[44]) Therefore, the combination of the HAADF pattern with the ABF pattern reveals the $Li_4Ti_5O_{12}$ structure on the atomic level, providing the possibility of shedding light on the Li storage and migration mechanism in this important anode material.

We next consider where the inserted ions are. **Figure 2** shows the static ABF images of different lithiated/delithiated

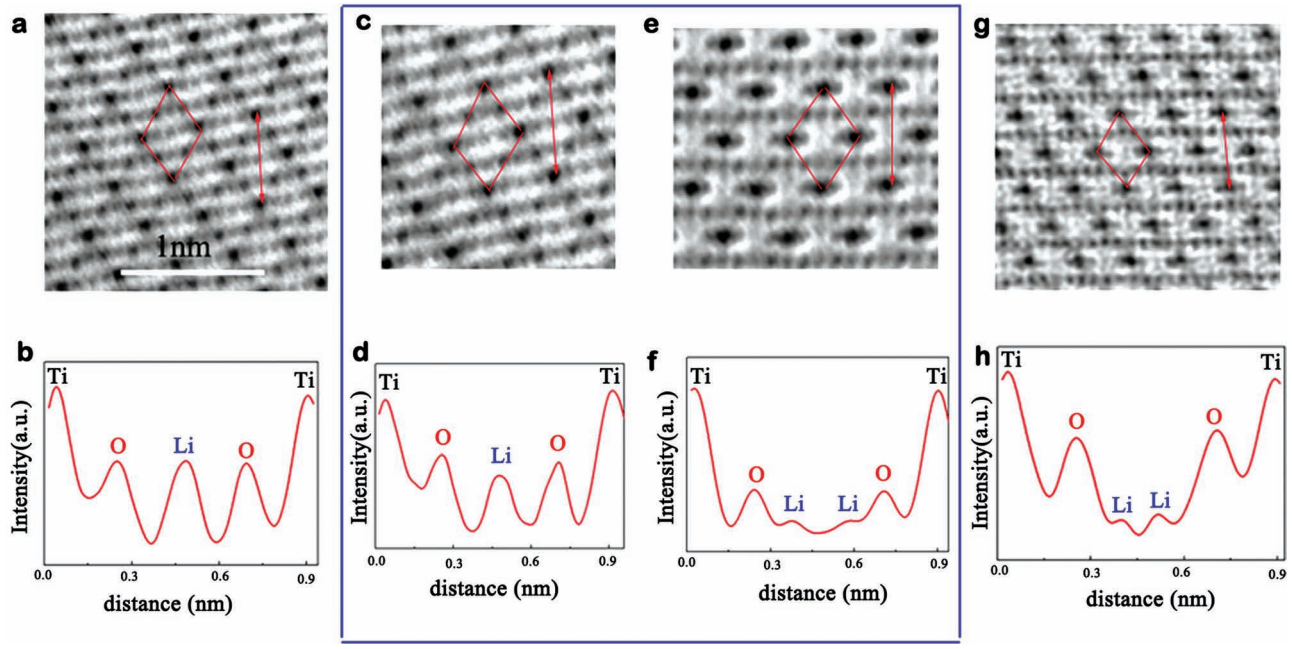

Figure 2. STEM ABF images of Li^+ ion insertion/extraction into/from $Li_4Ti_5O_{12}$ along the [110] zone axis. ABF images with line profiles of $Li_4Ti_5O_{12}$ with different lithiated/delithiated states: a,b) discharged to 1.0 V; c–f) charged to 85 mAh g^{-1}; g,h) charged to 2.2 V at the rate of C/20.

$Li_4Ti_5O_{12}$ electrodes. In contrast to Figure 1d, only one pronounced Li peak is found in Figure 2b after the $Li_4Ti_5O_{12}$ electrode has been discharged to 1.0 V. The two obvious Li 8a peaks in Figure 1d disappear. Here, from the evolution of peak intensity, it can be clearly deduced that during the formation of a single-phase $Li_7Ti_5O_{12}$, first, the intrinsic 8a Li^+ ions indeed migrate from the 8a sites to half of the 16c sites, and second, the excess Li^+ ions inserted are eventually stored in the other half of the 16c sites. These results are consistent with the finding from theoretical calculation that the configuration with all the Li^+ ions in the 16c sites has lower energy (Table S2 in the Supporting Information) than the situation where some Li^+ ions are in 8a sites.

In the half-delithiated state, two explicit regions, related to the $Li_4Ti_5O_{12}$ phase (Figures 2e,f) and the $Li_7Ti_5O_{12}$ phase (Figures 2c,d), are found in the ABF images. Only one peak, representing the 16c sites, is found in Figure 2d, indicating that the region shown in Figure 2c has taken on the structure of $Li_7Ti_5O_{12}$. In Figure 2f, two 8a Li^+ ion peaks are present and the 16c peak is absent, indicating $Li_4Ti_5O_{12}$ phase. Figures 2g and 2h show the $Li_4Ti_5O_{12}$ phase, which indicates that this mechanism is reversible. On charging, half of the 16c ions are extracted while the other half return to the 8a sites. The exact trajectory of these motions cannot be revealed by this static imaging technique, instead dynamic neutron diffraction or other suitable techniques are required.

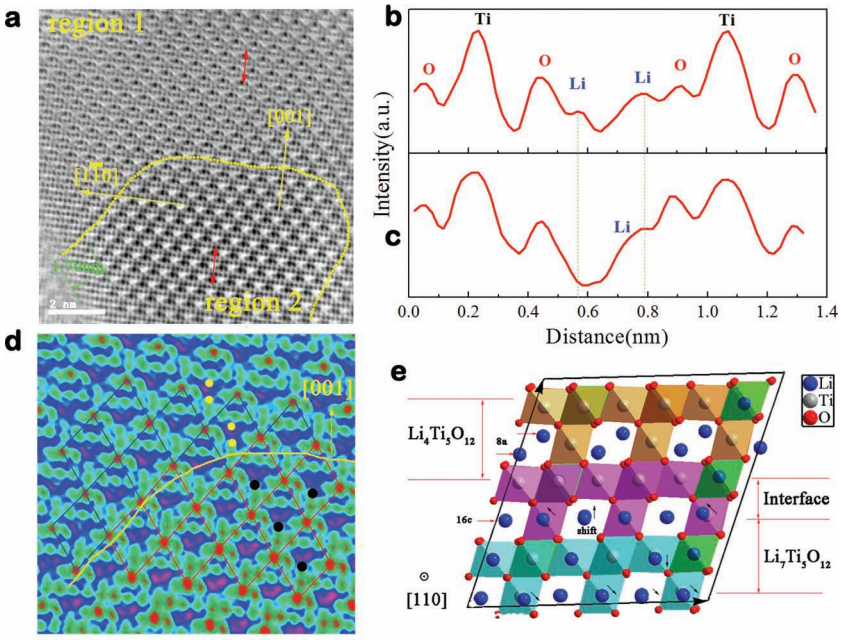

Figure 3. Interfacial structure in chemically lithiated $Li_4Ti_5O_{12}$ sample with about 0.15 mol Li insertion per formula unit along the [110] direction. a) ABF image near the interface between $Li_4Ti_5O_{12}$ phase (region 1) and $Li_7Ti_5O_{12}$ phase (region 2). The yellow line indicates the boundary of the interface. b) ABF line profile of region 1. c) ABF line profile of region 2. d) Colored ABF image of the two phases near the interface, where the 8a sites occupied in $Li_4Ti_5O_{12}$ and the 16c sites occupied in $Li_7Ti_5O_{12}$ are marked as yellow and black dots, respectively. e) The relaxed interfacial structure simulated by DFT calculations, where the Li_{16d}-O octahedrons are shown in green. The remarkable shifts of Li^+ ions at the 16c sites in the $Li_7Ti_5O_{12}$ region are indicated by black arrows.

We now turn to the interfacial structure. To the best of our knowledge, little attention has been paid in battery systems to the interfacial issues on the atomic scale. The best-studied system is probably $LiFePO_4$.[34,39,45] Among the many different observations, we mention just two: Chen et al. demonstrated that a pronounced dislocation region was observed by electron microscopy between the $LiFePO_4$ and $FePO_4$ regions in $Li_{0.5}FePO_4$ samples. This high dislocation density means that the phase boundary was highly disordered.[45] However, Gu et al., using a STEM technique, reported a staging phenomenon in $LiFePO_4$, characterized by alternation of fully occupied and empty layers along the [010] direction.[34] In the case of $Li_4Ti_5O_{12}$, the storage mechanism is still under dispute. It is rather generally accepted that the Li insertion/extraction process is a two-phase reaction.[18,20,25] However, Wagemaker et al. have shown by neutron diffraction that the two phases of interest in the lithiated material ($Li_{4+x}Ti_5O_{12}$), $Li_4Ti_5O_{12}$ and $Li_7Ti_5O_{12}$, appear to be unstable at room temperature and relax to a homogeneous solid solution but will separate into two phases again below 100 K.[7] In contrast, on a microscopic scale, a phase separation between Li-rich and Li-poor regions was indicated by NMR measurements.[12,13] So far, there has been no direct observation of the interfacial structure in lithiated $Li_4Ti_5O_{12}$, although a classic phase boundary movement is assumed.

As already observed above, two different phases are found in the half-charged state in electrochemically lithiated $Li_4Ti_5O_{12}$. Moreover, the $Li_4Ti_5O_{12}$ was chemically lithiated to $Li_{4+x}Ti_5O_{12}$ (x = 0.15; for the method see the Supporting Information), corresponding to the beginning of the two-phase region. Fortunately, the coexistence of the two phases in the surface region and bulk is clearly visible, as shown in **Figure 3**a and Figure S12 in the Supporting Information. From Figure 3b, it is obvious that the area of the $Li_4Ti_5O_{12}$ region (region 1) is larger than that of the $Li_7Ti_5O_{12}$ region (region 2), forming the main domains in the investigated particle. In Figure 3c, one of the 8a Li^+ ion peaks has totally disappeared while the other shows some displacement compared with Figure 3b (for a colored ABF image see Figure S11 in the Supporting Information) with the contrast of the Ti peaks being distinctly heightened. Therefore, this region 2 should correspond to the $Li_7Ti_5O_{12}$ phase with only one Li^+ ion peak in the 16c site although there is spatial fluctuation (region 2). The yellow curve in Figure 3a indicates the interface as a sharp phase boundary between the $Li_4Ti_5O_{12}$ and $Li_7Ti_5O_{12}$ phases in this two-phase reaction. Interestingly, this sharp phase boundary is also found in the interior region as shown in Figure S11 (Supporting Information).

A sharp phase boundary is, however, clearly found separating domains of $Li_4Ti_5O_{12}$ and $Li_7Ti_5O_{12}$ in Figure 3d, which is also supported by first-principles calculation as shown in Figure 3e. The calculation results indicate that Ti and O columns near the phase boundary stay almost the same as in $Li_4Ti_5O_{12}$. However, there is a pronounced 0.30 Å shift for the Li^+ ion from the 16c site (point 4 in Figure 1a) to the phase boundary in the $Li_7Ti_5O_{12}$

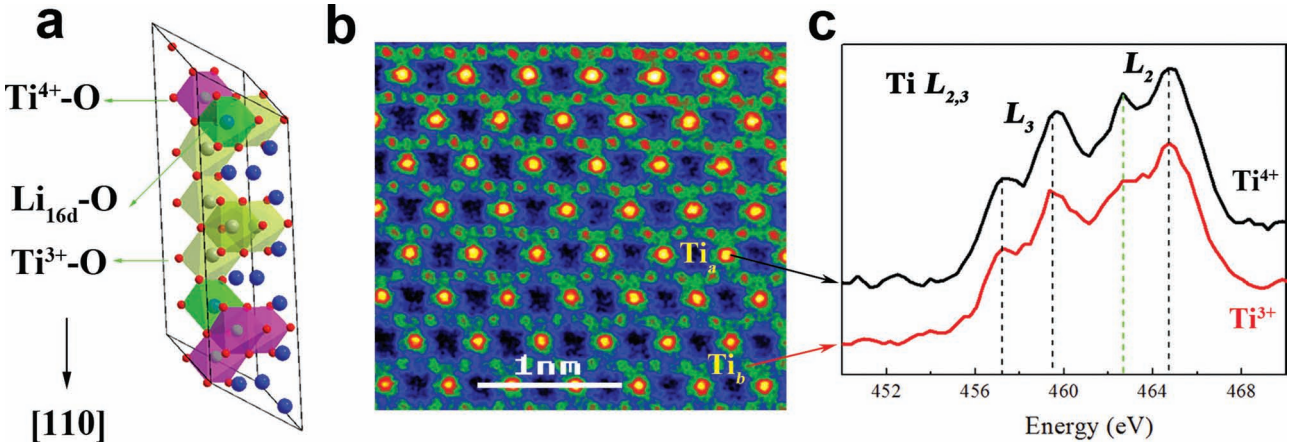

Figure 4. EELS profiles for Ti $L_{2,3}$ edges. a) Different chemical states of titanium sites, where the pink, yellow, and green colors correspond to the Ti^{4+}-O, Ti^{3+}-O and Li_{16d}-O octahedrons, respectively. The blue balls correspond to Li^+ in 16c sites. b) Color view of the enlarged STEM ABF image with different Ti columns. c) EELS profile Ti $L_{2,3}$ edges for the $Li_4Ti_5O_{12}$ electrode when discharged to 1.0 V taken from the two different Ti columns (indicated in (b)) along the [110] direction.

region as shown in Figure 3e (for the initial structure see Figure S16 in the Supporting Information). The shift is also found in the ABF image in the $Li_7Ti_5O_{12}$ region in Figures 3c,d. There is obvious consistency between the STEM observation and the calculations, both being in good agreement with the zero-strain characteristics during the lithiation/delithiation process.

Note that one of the contrasts of the oxygen columns in region 2 becomes significantly weaker in the inset of Figure S11b. The different contrast of the O columns is plausibly ascribed to the Ti–O bond distortion in the octahedron as a result of the excess electrons taking up the d-orbital of titanium on Li storage in $Li_4Ti_5O_{12}$ and/or to the energetic effects caused by interfacial Li^+ ion distribution, similar what was described by Borghols et al.[22]. Actually, this behavior elucidated by the STEM technique is also different from the core/shell model, where the Li-rich phase envelops the inner Li-poor core.

Finally, where are the inserted electrons? Previous theoretical results have revealed that the Ti ions are reduced from Ti^{4+} to $Ti^{3.4+}$ with Ti 3d orbitals partially occupied when $Li_4Ti_5O_{12}$ is fully lithiated.[24] As an average, this result is trivial, as it allocates three electrons stemming from three inserted Li. Our investigations achieve a more differentiated point of view and show that the valence is a spatial average over severe valence heterogeneities. **Figure 4** shows the corresponding electron energy-loss spectroscopy (EELS) results acquired with high spatial resolution for fully lithiated $Li_4Ti_5O_{12}$, that is, $Li_7Ti_5O_{12}$, in which the transfer of three electrons is achieved during the Li insertion. Being a fingerprint identification, Figure 4b shows the main peaks of Ti $L_{2,3}$ edges obtained by EELS for $Li_7Ti_5O_{12}$, which contain two main contributions from the L_2 and L_3 edges, split by the Ti 2p core–hole spin–orbit coupling of around 5 eV. The L_2 and L_3 edges are both subdivided into two edges by the strong crystal-field splitting due to the surrounding oxygen atoms. For Ti^{3+} ($3d^1$: $t_{2g}^1e_g^0$) ions, the EELS spectra indicate the electronic dipolar–allowed migration from the core-level Ti 2p to Ti $3d^{1+x}$ ($0 < x$, integer), but Ti 2p to Ti 3dx ($0 \le x$, integer) for Ti^{4+} ($3d^0$: $t_{2g}^0e_g^0$) ions. The spectrum taken from a Ti_a column shows Ti^{4+}-like characteristics, while Ti^{3+}-like features are found for the Ti_b columns.[27] It can be concluded that in the fully lithiated $Li_4Ti_5O_{12}$ the electrons are not homogenously distributed over the titanium orbitals and the Ti ions are in different valence states according to their local environment.

In order to understand the fundamental origin of the inhomogeneous charge distribution in $Li_7Ti_5O_{12}$, first-principles calculations were performed. The phase transformation from spinel to rock salt needs a six-electron transfer based on the supercell model (Figures S13–S16 in the Supporting Information). Bader atomic charge analyses for the Ti ions in the $Li_7Ti_5O_{12}$ supercell are presented in **Table 1**. In the table both the charge distribution around the Ti ions and the atomic volumes reveal clear differences, although the nearest distances still stay at the same level, leading to the zero-strain situation. In the GGA framework, an approximate average chemical state of the Ti ions indicates that the electrons are apt to delocalize as itinerant valence electrons. However, by modeling Ti 3d states as localized orbitals within the GGA+U approximation,

Table 1. Bader atomic charge analysis for the Ti ions in the $Li_7Ti_5O_{12}$ supercell, where charge distributions, the nearest atomic distances, and the atomic volumes are presented for GGA and GGA+U.

	GGA results			GGA+U (U_{eff} = 4.5 eV) results		
Ion	Charge [e]	d_{min} [nm]	Volume [Å^3]	Charge [e]	d_{min} [nm]	Volume [Å^3]
	1.4942	0.6708	4.2733	1.3829	0.6543	4.2011
	1.4991	0.6675	4.2945	1.3509	0.5418	4.0628
	1.5086	0.6735	4.2786	1.3837	0.6784	4.1683
	1.4962	0.6140	4.2562	1.3587	0.6556	4.0833
Ti	1.5625	0.6367	4.4928	1.7545	0.5730	5.6709
	1.5093	0.6735	4.2548	1.7483	0.6073	5.7093
	1.6226	0.6170	4.6963	1.7554	0.6174	5.5682
	1.6282	0.6722	4.7769	1.7522	0.6456	5.6065
	1.5760	0.6587	4.6064	1.7595	0.6315	5.7271
	1.5760	0.6805	4.8047	1.7765	0.6328	5.7106

the charges of Ti separate into two types (Table 1), which can be assigned as Ti^{3+} -like and Ti^{4+}-like, as observed in the EELS experiments. No evidence for the average chemical state of Ti ions in $Li_7Ti_5O_{12}$ is found. However, the various distributions of Li^+ ions at the 16d sites affect the Ti^{3+}/Ti^{4+}-like patternings greatly (Figures S17–S19 in the Supporting Information), suggesting a strong coupling between the charge state of Ti and the distribution of Li. This confirms the assumption of strong Li^+–e^- association. According to the spin charge density integration results (Figure S20, Supporting Information) by GGA+U, the excess electrons from the inserted Li are localized around the Ti_a 3d orbitals obviously and the net magnetic moment is 2.99 μ_B per formula unit (where μ_B is the Bohr magneton), which is ascribed to the excess three electrons from the inserted Li. Therefore, the results by the GGA+U method give a proper description of the EELS experimental results.

In conclusion, an aberration-corrected STEM technique has been employed in combination with theoretical calculations to study Li storage in the $Li_4Ti_5O_{12}$ lattice. The STEM ABF images clearly demonstrated that in addition to the variation of the lithium content, the Li ions change site on lithiation/delithiation, with Li^+ ions occupying only the 8a sites in $Li_4Ti_5O_{12}$ and occupying only the 16c sites in $Li_7Ti_5O_{12}$. The corresponding interfacial structure was also visualized in the surface and bulk of the chemically lithiated $Li_4Ti_5O_{12}$ sample and was found to be a sharp coherent heterophase. Furthermore, EELS analysis showed that the Ti ions adopt locally different valences upon lithiation according to the picture of strong Li^+–e^- association, which is also in accordance with the GGA+U DFT calculation. So, the full static picture has been resolved and the following questions answered: i) Where are the excess Li ions after lithiation? ii) Where are the excess electrons? iii) What is the shape of the interface?

Experimental Section

Aberration-corrected STEM was performed using a JEOL 2100F (JEOL, Tokyo) transmission electron microscope equipped with a CEOS (CEOS, Heidelberg, Germany) probe aberration corrector. The calculations were performed by the Vienna ab initio simulation package (VASP). For experimental and calculation details see the Supporting Information.

Supporting Information

Supporting Information is available from the Wiley Online Library or from the author.

Acknowledgements

The authors thank Prof. Xuejie Huang, Prof. Chuying Ouyang and Mr. Yang Sun for fruitful discussions. This work was supported by funding from the "863" Project (2009AA033101), "973" Projects (2009CB220104, 2010CB833102), NSFC (50972164), CAS project (KJCX2-YW-W26) and One Hundred Talent Project of the Chinese Academy of Sciences. The calculations were finished at the Virtual Laboratory for Computational Chemistry, Computer NetWork Information Center, Chinese Academy of Sciences.

Received: February 1, 2012
Revised: March 21, 2012
Published online: May 16, 2012

[1] P. G. Bruce, B. Scrosati, J. M. Tarascon, *Angew. Chem. Int. Ed.* **2008**, *47*, 2930.
[2] V. Etacheri, R. Marom, R. Elazar, G. Salitra, D Aurbach, *Energy Environ. Sci.* **2011**, *4*, 3243.
[3] W. Dreyer, J. Jamnik, C. Guhlke, R. Huth, J. Moskon, M. Gaberscek, *Nat. Mater.* **2010**, *9*, 448.
[4] A. Deschanv, B. Raveau, Z. Sekkal, *Mater. Res. Bull.* **1971**, *6*, 699.
[5] E. Ferg, R. J. Gummow, A. Dekock, M. M. Thackeray, *J. Electrochem. Soc.* **1994**, *141*, L147.
[6] T. Ohzuku, A. Ueda, N. Yamamoto, *J. Electrochem. Soc.* **1995**, *142*, 1431.
[7] M. Wagemaker, D. R. Simon, E. M. Kelder, J. Schoonman, C. Ringpfeil, U. Haake, D. Lutzenkirchen-Hecht, R. Frahm, F. M. Mulder, *Adv. Mater.* **2006**, *18*, 3169.
[8] L. Zhao, Y. S. Hu, H. Li, Z. X. Wang, L. Q. Chen, *Adv. Mater.* **2011**, *23*, 1385.
[9] G.-N. Zhu, H.-J. Liu, J.-H. Zhuang, C.-X. Wang, Y.-G. Wang, Y.-Y. Xia, *Energy Environ. Sci.* **2011**, *4*, 4016.
[10] L. Cheng, J. Yan, G. N. Zhu, J. Y. Luo, C. X. Wang, Y. Y. Xia, *J. Mater. Chem.* **2010**, *20*, 595.
[11] Z. L. Jian, L. Zhao, R. Wang, Y.-S. Hu, H. Li, W. Chen, L. Q. Chen, *RSC Adv.* **2012**, *2*, 1751.
[12] M. Wilkening, W. Iwaniak, J. Heine, V. Epp, A. Kleinert, M. Behrens, G. Nuspl, W. Bensch, P. Heitjans, *Phys. Chem. Chem. Phys.* **2007**, *9*, 6199.
[13] M. Wagemaker, E. R. H. van Eck, A. P. M. Kentgens, F. M. Mulder, *J. Phys. Chem. B* **2009**, *113*, 224.
[14] Z. J. Ding, L. Zhao, L. M. Suo, Y. Jiao, S. Meng, Y.-S. Hu, Z. X. Wang, L. Q. Chen, *Phys. Chem. Chem. Phys.* **2011**, *13*, 15127.
[15] H. L. Pan, Y.-S. Hu, H. Li, L. Q. Chen, *Chin. Phys. B* **2011**, *20*, 118202.
[16] H. L. Pan, L. Zhao, Y.-S. Hu, H. Li, L. Q. Chen, *ChemSusChem.* **2012**, *5*, 526.
[17] M. M. Rahman, J. Z. Wang, M. F. Hassan, D. Wexler, H. K. Liu, *Adv. Energy Mater.* **2011**, *1*, 212.
[18] Y. Wang, H. Liu, K. Wang, H. Eiji, Y. Wang, H. Zhou, *J. Mater. Chem.* **2009**, *19*, 6789.
[19] L. Zhao, H. L. Pan, Y.-S. Hu, H. Li, L. Q. Chen, *Chin. Phys. B* **2012**, *21*, 028201.
[20] A. S. Prakash, P. Manikandan, K. Ramesha, M. Sathiya, J. M. Tarascon, A. K. Shukla, *Chem. Mater.* **2010**, *22*, 2857.
[21] H. G. Jung, S. T. Myung, C. S. Yoon, S. B. Son, K. H. Oh, K. Amine, B. Scrosati, Y. K. Sun, *Energy Environ. Sci.* **2011**, *4*, 1345.
[22] W. J. H. Borghols, M. Wagemaker, U. Lafont, E. M. Kelder, F. M. Mulder, *J. Am. Chem. Soc.* **2009**, *131*, 17786.
[23] K. Amine, I. Belharouak, Z. H. Chen, T. Tran, H. Yumoto, N. Ota, S. T. Myung, Y. K. Sun, *Adv. Mater.* **2010**, *22*, 3052.
[24] C. Y. Ouyang, Z. Y. Zhong, M. S. Lei, *Electrochem. Commun.* **2007**, *9*, 1107.
[25] S. Scharner, W. Weppner, P. Schmid-Beurmann, *J. Electrochem. Soc.* **1999**, *146*, 857.
[26] Z. L. Zhang, W. Sigle, F. Phillipp, M. Rühle, *Science* **2003**, *302*, 846.
[27] S.-H. Yang, L. Croguennec, C. Delmas, E. C. Nelson, M. A. O'Keefe, *Nat. Mater.* **2003**, *2*, 464.
[28] D. A. Muller, N. Nakagawa, A. Ohtomo, J. L. Grazul, H. Y. Hwang, *Nature* **2004**, *430*, 657.
[29] L. Fitting, S. Thiel, A. Schmehl, J. Mannhart, D. A. Muller, *Ultramicroscopy* **2006**, *106*, 1053.
[30] S. Y. Chung, S. Y. Choi, T. Yamamoto, Y. Ikuhara, *Phys. Rev. Lett.* **2008**, *100*, 125502.
[31] Y. Oshima, H. Sawada, F. Hosokawa, E. Okunishi, T. Kaneyama, Y. Kondo, S. Niitaka, H. Takagi, Y. Tanishiro, K. Takayanagi, *J. Electron. Microsc.* **2010**, *59*, 457.
[32] S. D. Findlay, T. Saito, N. Shibata, Y. Sato, J. Matsuda, K. Asano, E. Akiba, T. Hirayama, Y. Ikuhara, *Appl. Phys. Express* **2010**, *3*, 116603.

[33] R. Ishikawa, E. Okunishi, H. Sawada, Y. Kondo, F. Hosokawa, E. Abe, *Nat. Mater.* **2011**, *10*, 278.
[34] L. Gu, C. B. Zhu, H. Li, Y. Yu, C. L. Li, S. Tsukimoto, J. Maier, Y. Ikuhara, *J. Am. Chem. Soc.* **2011**, *133*, 4661.
[35] R. Huang, Y. H. Ikuhara, T. Mizoguchi, S. D. Findlay, A. Kuwabara, C. A. J. Fisher, H. Moriwake, H. Oki, T. Hirayama, Y. Ikuhara, *Angew. Chem. Int. Ed.* **2011**, *50*, 3053.
[36] R. Huang, T. Hitosugi, S. D. Findlay, C. A. J. Fisher, Y. H. Ikuhara, H. Moriwake, H. Oki, Y. Ikuhara, *Appl. Phys. Lett.* **2011**, *98*, 051913.
[37] X. Lu, Z. L. Jian, Z. Fang, L. Gu, Y. S. Hu, W. Chen, Z. X. Wang, L. Q. Chen, *Energy Environ. Sci.* **2011**, *4*, 2638.
[38] R. Huang, Y. Ikuhara, *Curr. Opin. Solid State Mater. Sci.* **2012**, *16*, 31.
[39] L. M. Suo, W. Z. Han, X. Lu, L. Gu, Y.-S. Hu, H. Li, D. F. Chen, L. Q. Chen, S. Tsukimoto, Y. Ikuhara, *Phys. Chem. Chem. Phys.* **2012**, *14*, 5363.
[40] J. Maier, R. Amin, *J. Electrochem. Soc.* **2008**, *155*, A339.
[41] C. L. Olson, J. Nelson, M. S. Islam, *J. Phys. Chem. B* **2006**, *110*, 9995.
[42] S. D. Findlay, N. Shibata, H. Sawada, E. Okunishi, Y. Kondo, T. Yamamoto, Y. Ikuhara, *Appl. Phys. Lett.* **2009**, *95*, 191913.
[43] S. D. Findlay, N. Shibata, H. Sawada, E. Okunishi, Y. Kondo, Y. Ikuhara, *Ultramicroscopy* **2010**, *110*, 903.
[44] A. Du Pasquier, I. Plitz, S. Menocal, G. Amatucci, *J. Power Sources* **2003**, *115*, 171.
[45] G. Y. Chen, X. Y. Song, T. J. Richardson, *Electrochem. Solid State Lett.* **2006**, *9*, A295.